Electronic Supplementary Material (ESI) for Physical Chemistry Chemical Physics

SUPPORTING INFORMATION

Critical Role of Small Micropores in High CO_2 Uptake

By *Zhongshen Zhang,*[a] *Jin Zhou,*[a] *Wei Xing,* *[a, b] *Qingzhong Xue,*[b] *Zifeng Yan,*[b] *Shuping Zhuo**[a] *and Shi Zhang Qiao**[c]

Z. Zhang and J. Zhou made equal contributions to this work.

[a] School of Chemical Engineering, Shandong University of Technology
Zibo 255049 (P. R. China)
E-mails: xwcatalysis@gmail.com; zhuosp_academic@yahoo.com

[b] State Key Laboratory of Heavy Oil Processing
School of Science, China University of Petroleum
66 Changjiang West Road, Qingdao 266580 (P. R. China)

[c] *School of Chemical Engineering*
The University of Adelaide, SA5005 (Australia)
Email: s.qiao@adelaide.edu.au

Caption of Tables and Figures

Table S1 Pore structure parameters of the carbon samples

Table S2 N-containing groups on the surface of the prepared carbons

Table S3 CO_2 uptake comparison of various porous carbon materials at 25 °C

Table S4 CO_2 uptake comparison of various porous carbons at 75 °C

Fig. S1 SEM (a-d) and TEM (e-h) images of the prepared carbons: (a) PANI, (b) PC, (c) AC-700-2, (d) AC-800-0.5, (e) AC-600-0.5, (f) AC-800-1, (g) AC-700-0.5 and (h) AC-700-2

Fig. S2 N_2 sorption isotherms of the prepared carbons

Fig. S3 Pore size distributions of the prepared carbons

Fig. S4 N1s spectra: (a) AC-600-2, (b) AC-700-1, (c) AC-700-2 and (d) AC-800-1

Fig. S5 Fourier-transform infrared (FTIR) spectra of the obtained carbons

Fig. S6 Comparison of CO_2 (● in red) and N_2 (■ in black) sorption profiles at 25 °C. (a) AC-600-0.5, (b) AC-700-0.5, (c) AC-750-0.5, (d) AC-800-0.5

Fig. S7 (a) Cycles of CO_2 sorption at 25 °C, (b) The time to reach adsorption equilibrium at different terminal pressure (25 °C) for AC-750-0.5

Fig. S8 The correlation of adsorption data measured at 25 °C with Langmuir equation

Fig. S9 The correlation of CO_2 adsorption data measured at 25 °C with D-A model

Fig. S10 CO_2 adsorption in different-sized pores

Fig. S11 The prediction of the CO_2 uptake on the investigated carbons at 25 °C

Fig. S12 The curves of sorption potential energy in different-sized micropores

Fig. S13 The plots of Q_{st} vs. CO_2 sorption pressure at 25 °C

Table S1 Pore structure parameters of the carbon samples

Samples	Pore structure parameters			
	S_{BET}[a] ($m^2\ g^{-1}$)	V_{total}[b] ($cm^3\ g^{-1}$)	V_{micro}[c] ($cm^3\ g^{-1}$)	D[d] (nm)
AC-600-0.5	508	0.31	0.24	2.55
AC-600-1	905	0.52	0.44	2.28
AC-600-2	966	0.59	0.45	2.45
AC-700-0.5	826	0.51	0.40	2.45
AC-700-1	1685	0.94	0.82	2.23
AC-700-2	1920	1.10	0.90	2.28
AC-800-0.5	1244	0.73	0.60	2.33
AC-800-1	2448	1.39	0.99	2.34
AC-800-2	2994	1.94	0.48	2.49
AC-750-0.5	1091	0.61	0.5	2.27
AC-600-0.5-H[e]	404	0.23	0.19	2.31

[a]BET specific surface area. [b]Single point total pore volume measured at P/P_0 = 0.995. [c]Micropore volume calculated by modern NLDFT method. [d]Average pore size calculated by $4V_{total}/S_{BET}$. [e]This sample was obtained by heat-treating AC-600-0.5 at 800 °C for 1 hour under N_2 atmosphere.

Table S2 N-containing groups on the surface of the prepared carbons

Table	N content (wt%)	Pyridinic-N (%)	-C=NH (%)	Pyrrolic-N (%)	Quaternary-N (%)
AC-600-0.5	6.7	17.74	19.41	37.23	25.61
AC-600-2	4.5	14.35	20.57	36.19	28.89
AC-700-0.5	6.6	12.78	19.36	27.89	39.97
AC-700-1	2.7	11.1	20.62	26.96	41.32
AC-700-2	2.8	10.95	23.15	23.23	42.67
AC-800-0.5	3.3	9.04	21.63	21.63	47.71
AC-800-1	3.9	6.46	21.53	15.66	56.36
AC-600-0.5-H	3.2	4.81	27.15	8.84	59.21

Table S3 CO_2 uptake comparison of various porous carbon materials at 25 °C

Materials	CO_2 uptake (mmol g^{-1})		Reference
	1 bar	0.15 bar	
AC-750-0.5	4.30	1.38	This study
activated carbon (S_{BET} = 2829 m^2 g^{-1})	2.92	N.A.	29
KOH-activated graphite nanofibers	1.35	<0.5	22
KOH-activated templated carbons	3.4	<1.0	23
KOH-activated polypyrrole	3.9	~1.0	26
activated urea-formaldehyde resin	1.86	N.A.	27
N-doped porous carbon monoliths	3.13	N.A.	28
NAC	3.75	N.A.	29
porous carbon nitride spheres	2.90	N.A.	30
carbon from bean dreg	4.24	1.2	37
carbon from poly(benzoxazine-co-resol)	3.3	1.0	38
N-doped ZTCs	4.38	<1.0	39
Fungi-based carbons	3.5	~1.0	41
activated anthracites	1.49	N.A.	42
ammonia-treated carbons	2.2	N.A.	43
activated melamine–formaldehyde resin	2.25	N.A.	44
Hydrothermally treated biomass	4.8	~1.2	20
IBN9-NC1-A	4.50	N.A.	45

Table S4 CO_2 uptake comparison of various porous carbons at 75 °C

Materials	CO_2 uptake (mmol g^{-1})	Reference
AC-750-0.5	1.86	This study
activated urea-formaldehyde resin	0.81	27
N-doped porous carbon monoliths	1.5 (at 60 °C)	28
KOH-activated polypyrrole	1.7 (at 50 °C)	26
porous carbon nitride spheres	0.97	30
activated anthracites	0.57	42
ammonia-treated carbons	0.73	43
activated melamine–formaldehyde resin	0.86	44

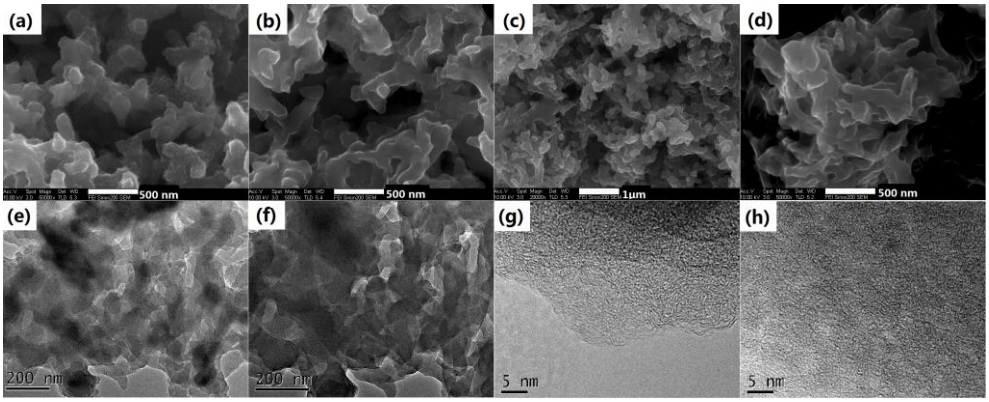

Fig. S1 SEM (a-d) and TEM (e-h) images of the prepared carbons: (a) PANI, (b) PC, (c) AC-700-2, (d) AC-800-0.5, (e) AC-600-0.5, (f) AC-800-1, (g) AC-700-0.5 and (h) AC-700-2

The PANI particles form nanofibrillar agglomerates with ~200 nm in diameter and ~1 μm in length (Fig. S1a). The carbonaceous residual (PC) obtained by pre-carbonization of PANI still exhibits a rod-like structure, and the diameter is smaller than that of the pristine PANI due to shrinkage of PANI during the carbonization progress (Fig. S1b). This carbonaceous residual possesses a relative high surface area (117 m^2 g^{-1} derived from N_2 sorption) which offers a large interfacial area for the impregnation of KOH. Macropores are observed in the TEM images of AC-600-0.5 and AC-800-1 (Fig. S1e, f). These macropores maybe inherit from the morphology of the polymer PANI and are maintained during the carbonization process. HR-TEM images (Fig. S1g, h) clearly present that worm-like micropores are formed by the stacking of curved graphene layers in the prepared carbons. The sizes of most micropores are less than 1 nm.

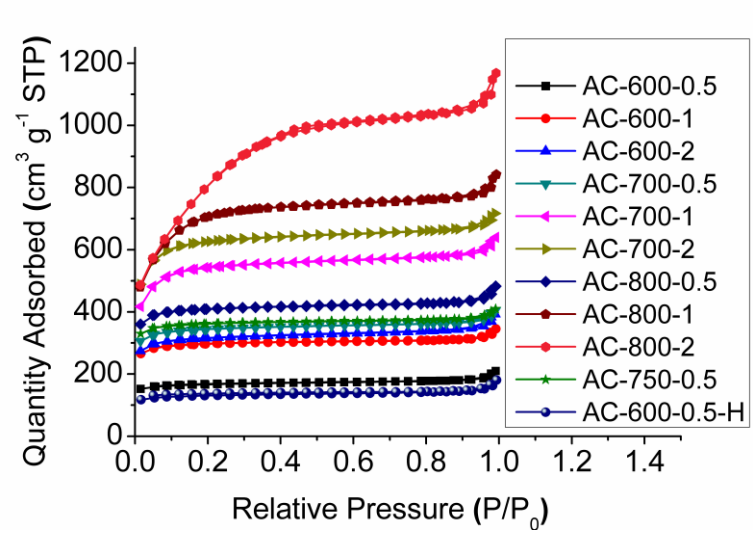

Fig. S2 N_2 sorption isotherms of the prepared carbons

N_2 sorption isotherms of the prepared carbons (Fig. S2) gradually shift upwards with the increase of KOH dosage and activation temperature, indicating the increase of porosity. All the carbons (except AC-800-2) present an isotherm of type I, which rapidly achieve a high adsorption plateau at very low relative pressure, indicating microporous nature of these carbons. The adsorption amounts of these carbons do not increase further until a relative pressure higher than 0.9, and no hysteresis loop in medium relative pressure (0.3-0.8) is found, indicating the absence of mesopores. In contrast, AC-800-2 shows a rising of adsorption amount in relative pressure ranging from 0.3 to 0.6, suggesting that mesopores are produced due to over-activation at large KOH dosage and high activation temperature. All the isotherms emerge an upswept rear edge at high relative pressure (>0.9), suggesting the existence of macropores.

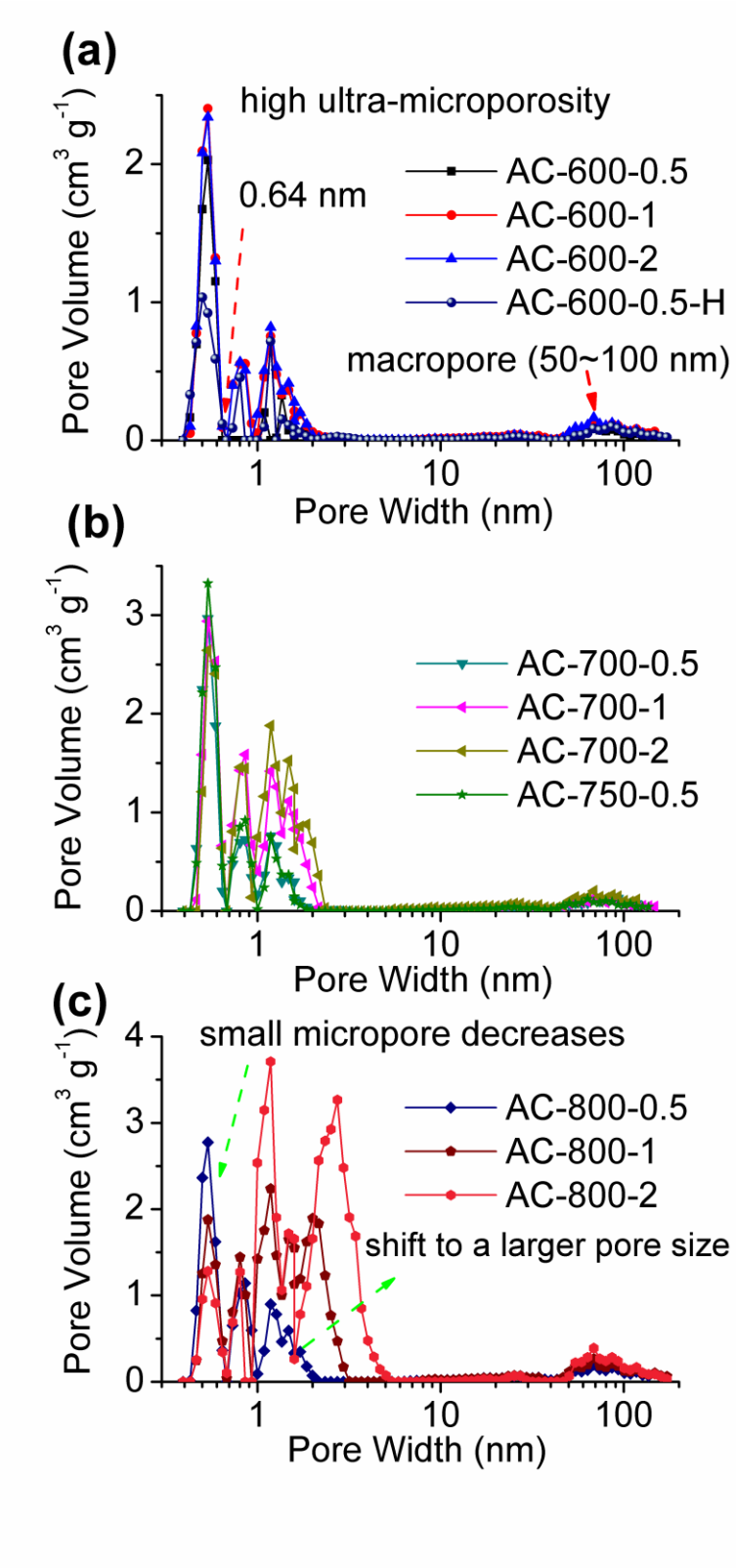

Fig. S3 Pore size distributions of the prepared carbons

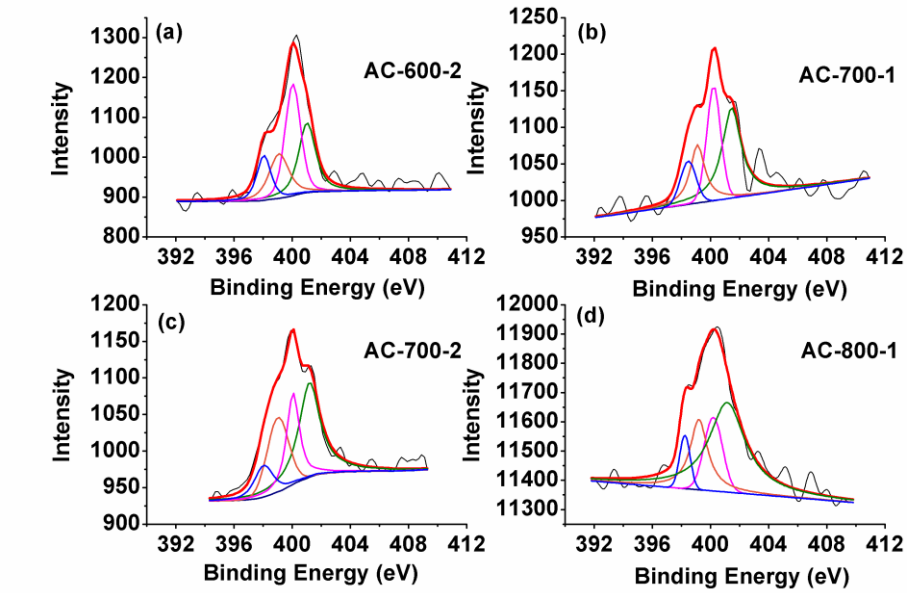

Fig. S4 N1s spectra: (a) AC-600-2, (b) AC-700-1, (c) AC-700-2 and (d) AC-800-1

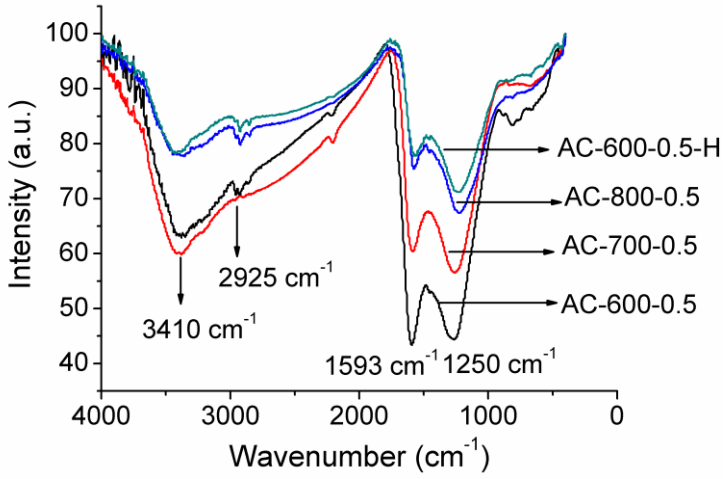

Fig. S5 Fourier-transform infrared (FTIR) spectra of the obtained carbons

Fourier-transform infrared (FTIR) spectroscopy (Fig S5) was employed to further confirm the surface chemical properties of the obtained carbons. The peak at about 3410 cm^{-1} can be assigned to the N-H symmetric stretching vibration. The peaks at around 2800-3000 cm^{-1} indicate the presence of the C-H stretching vibration. The medium strong peak at about 1593 cm^{-1} is attributed to C=C stretching vibration. The strong peak around 1250 cm^{-1} is assigned to the C-N stretching vibration. The bands between 950 and 650 cm^{-1} correspond to the

out-of-plane N-H deformation vibration. The FTIR analysis suggests that N–H and C–N species are present in the samples. Generally, higher carbonization temperature would result in decrease of hetero-atoms like N, H, O. According to FTIR, N-H in-plane deformation vibrations and C-N stretching vibration peaks overlap and their intensity decreases with the increase of activation temperature, according with the results of XPS measurements.

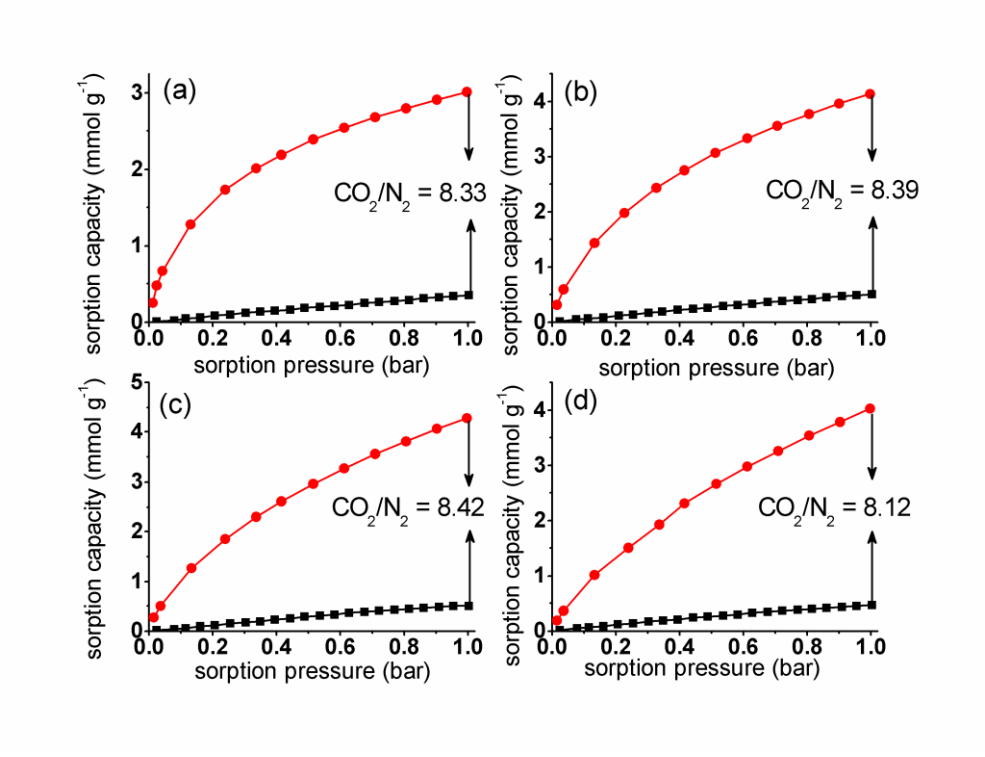

Fig. S6 Comparison of CO_2 (● in red) and N_2 (■ in black) sorption profiles at 25 ^{o}C. (a) AC-600-0.5, (b) AC-700-0.5, (c) AC-750-0.5, (d) AC-800-0.5

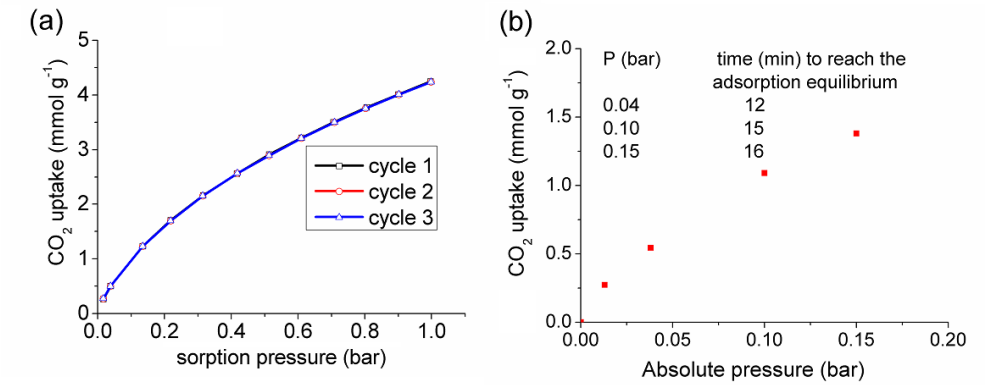

Fig. S7 (a) Cycles of CO_2 sorption at 25 °C, (b) The time to reach adsorption equilibrium at different terminal pressure (25 °C) for AC-750-0.5

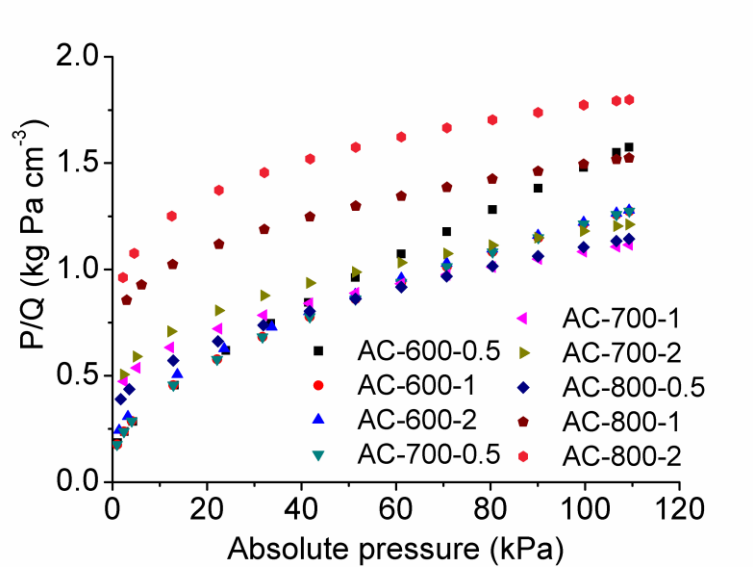

Fig. S8 The correlation of adsorption data measured at 25 °C with Langmuir equation

In order to reveal the adsorption mechanism, the isotherms are simulated using two different adsorption models including Langmuir and Dubinin-Astakhov (D-A) models (Fig. S6, S7).

The well-known Langmuir isotherm model can be expressed by equation 1.

$$\frac{Q}{Q_0} = \frac{bP}{1+bP} \tag{1}$$

where Q (cm^{-3} g^{-1}) denotes the amount adsorbed, Q_0 (cm^3 g^{-1}) denotes the saturated amount adsorbed, P (kPa) denotes the equilibrium pressure, and b/kP^{-1} denotes the adsorption affinity. A linear expression for the Langmuir equation is

$$\frac{P}{Q} = \frac{1}{bQ_0} + \frac{1}{Q_0}P \tag{2}$$

Fig. S6 shows the correlation of adsorption data with Langmuir equation. It could be clearly found that the CO_2 adsorption isotherms cannot be well fitted by the Langmuir model.

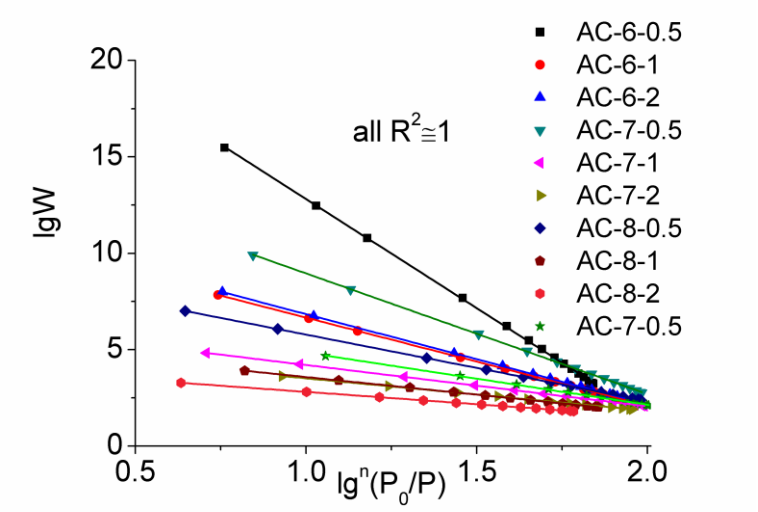

Fig. S9 The correlation of CO_2 adsorption data measured at 25 °C with D-A model

Dubinin-Astakhov (D-A) model is applied to the adsorption equilibrium of CO_2 onto the activated carbons. D-A equation is written as

$$W = W_0 \exp\left[-\left(\frac{A}{E}\right)^n\right] \tag{3}$$

$$\ln W = \ln W_0 - (\frac{A}{E})^n \tag{4}$$

where W denotes the volume adsorbed, W_0 denotes the limiting micropore volume, E denotes the characteristic energy of the system, n denotes the heterogeneity parameter, and A denotes the adsorption potential. The adsorption potential A is given by

$$A = RT \ln(\frac{P_0}{P}) \tag{5}$$

where R is the gas constant, T is the equilibrium temperature, and P_o is the saturated pressure. Then the D-A equation could be expressed as

$$\ln W = \ln W_0 - (\frac{RT}{E})^n \ln^n(\frac{P_0}{P}) \tag{6}$$

$$\lg W = \lg W_0 - \left[2.303^{n-1}(\frac{RT}{E})^n\right] \lg^n(\frac{P_0}{P}) \tag{7}$$

A plot of lgW versus $\lg^n(\frac{P_0}{P})$ should give a straight line with a slope of $-[2.303^{n-1}(\frac{RT}{E})^n]$ and an intercept of lgW_0 if the adsorption isotherms fit well the D-A model.

Apparently, the experimental data can be well fitted by the D-A equation (Fig. S7). The simulation results indicate that the CO_2 adsorption on the porous carbons can be well depicted by a micropore filling mechanism, not by monolayer adsorption.

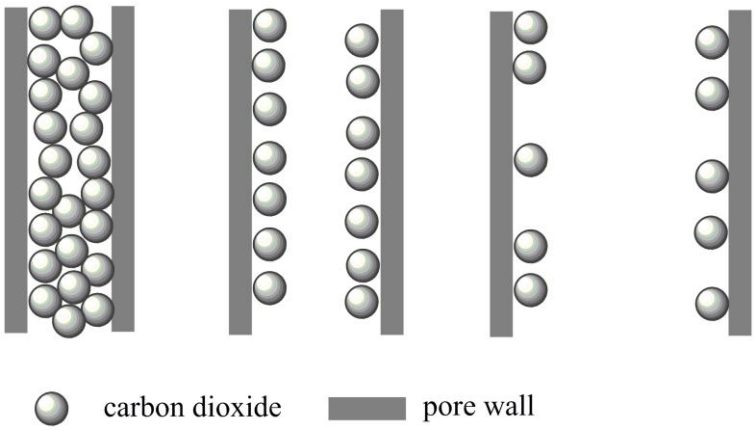

Fig. S10 CO_2 adsorption in different-sized pores

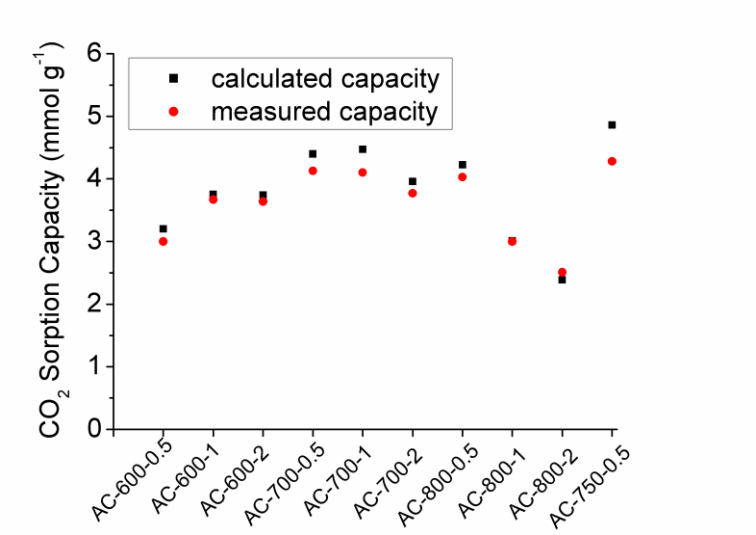

Fig. S11 The prediction of the CO_2 uptake on the investigated carbons at 25 °C

The theoretical CO_2 adsorption capacity at 25 °C is calculated by multiplying the density of CO_2 at 25 °C (0.705 g cm^{-3}) by micropore volume (pore size < 0.70 nm) of samples. The measured capacity is obtained from CO_2 sorption isotherms. It could be seen that these two series of capacities are much closed although the investigated carbons possess much different N content (Fig. S11). This result indicated that the small micropore is dominant to the CO_2 uptake and the N-content does not enhance CO_2 capture capacities obviously.

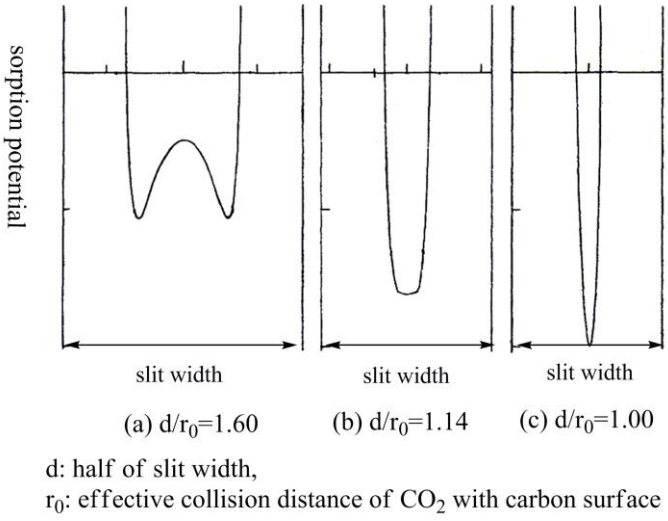

Fig. S12 The curves of sorption potential energy in different-sized micropores

The CO_2 sorption potential energy curves in three representative micropores are displayed in Fig. S12. The slit width is the distance between the two graphite lattice planes of slit pore walls. The r_0 value (the effective collision distance of CO_2 with carbon surface) is equal to the sum of molecule radius of CO_2 and interlayer spacing of graphite planes, about 0.33 nm. Obviously, the slit width is larger than the available pore width (i.e. pore size measured by gas sorption) due to the pristine interlayer space of graphite plane. The micropores in carbons possess high adsorption potential due to the superposition of the van der Waals force given by two adjacent walls of slit pores. With the decrease of the pore width, the superposition extent of the van der Waals force increases, resulting in the rise of adsorption potential (Fig. S12). For extremely small micropores (Fig. S12c), the potential energy curve exhibits a single minimum with increasing depth of potential well (about double of sorption potential derived from each pore wall) and sharpening curvature due to the entire superposition of the van der Wall force derived from the two adjacent walls of slit pores, indicating that these pores strongly interact with CO_2 molecules and could lead to higher adsorption heats. The critical state (Fig. S12b) is that the double minima of adsorption potential merge into a single minimum. According to Everett's report[1], the pore width at this critical state is about 0.54 nm (corresponding to slit width of about 0.76 nm), strictly consistent with the experimental value of this work (Fig. 4h). For the micropores larger than 0.54 nm, the adsorption potential

significantly decreases due to the much lower superposition extent of the sorption potential, leading to weak interaction between CO_2 and carbon adsorbent.

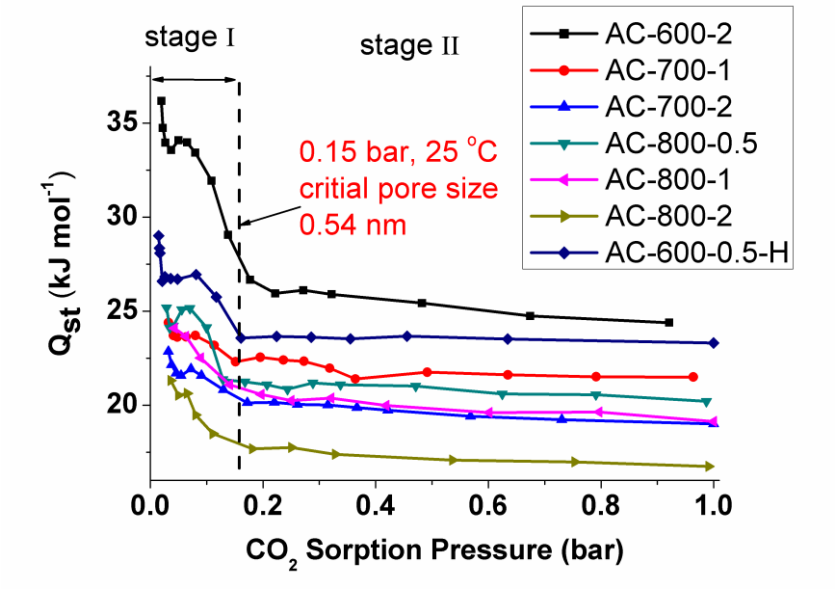

Fig. S13 The plots of Q_{st} vs. CO_2 sorption pressure at 25 °C

The isosteric heats of adsorption (Q_{st}) were calculated according to Clausius-Clapeyron equation:

$$\ln\left(\frac{p_1}{p_2}\right) = Q_{st} \times \frac{T_2 - T_1}{R \times T_1 \times T_2} \tag{8}$$

where Q_{st} is the isosteric heats of adsorption, T_i represents a temperature at which an isotherm i is measured, p_i represents a pressure at which a specific equilibrium adsorption amount is reached at T_i, R is gas constant (8.314 J/(K mol^{-1})). The Q_{st} of the prepared carbons decreases with increasing of CO_2 sorption pressure (Fig. S13). Most of the carbons display a typical two-stage curve of Q_{st}, and the Q_{st} shows a significant drop in the stage II of Q_{st} curves. At the outset of stage II in Q_{st} curves, the corresponding sorption condition is 0.15 bar and 25 °C. As discussed in Fig. 4h, the CO_2 uptake at 0.15 bar and 25 °C for the investigated carbons is achieved by the micropores smaller than 0.54 nm. Thus, we can conclude that 0.54 nm is a critical pore size value corresponding to the outset of stage II in Q_{st} curves.

Calculation of coefficient of determination (R^2)

The coefficient of determination, R^2, was calculated by the equation

$$R^2 = 1 - \frac{\sum_{i=1}^{n} (y_i - f(x_i))^2}{\sum_{i=1}^{n} (y_i - \bar{y})^2} \quad (9)$$

where y_i is the i^{th} measured data, $f(x_i)$ is the predicted value derived from a linear equation, and $\bar{y}$ is the mean of the measured data. R^2 is a statistic that will give some information about the goodness of a model fitting. In regression, the coefficient of determination, R^2, is a statistical measure of how well the regression line approximates the real data points. Specifically, R^2 is an element of [0, 1]. A higher R^2 (closed to 1.0) indicates that the regression line well fits the data, while a lower R^2 (near 0) indicates no 'linear' relationship between the response variable and regressor.

Reference

1 D. H. Everett and J. C. Powl, *J. Chem. Soc., Faraday Trans.*, 1976, 72, 619-636.